Spinor Dynamics in an Antiferromagnetic Spin-1 Condensate

A. T. Black, E. Gomez, L. D. Turner, S. Jung, and P. D. Lett

Joint Quantum Institute, University of Maryland and National Institute of Standards and Technology, Gaithersburg, Maryland 20899, USA

(Received 6 April 2007; revised manuscript received 8 June 2007; published 16 August 2007)

We observe coherent spin oscillations in an antiferromagnetic spin-1 Bose-Einstein condensate of sodium. The variation of the spin oscillations with magnetic field shows a clear signature of nonlinearity, in agreement with theory, which also predicts anharmonic oscillations near a critical magnetic field. Measurements of the magnetic phase diagram agree with predictions made in the approximation of a single spatial mode. The oscillation period yields the best measurement to date of the sodium spin-dependent interaction coefficient, determining that the difference between the sodium spin-dependent s-wave scattering lengths $a_{f=2} - a_{f=0}$ is 2.47 ± 0.27 Bohr radii.

DOI: 10.1103/PhysRevLett.99.070403 PACS numbers: 05.30.Jp, 03.75.Mn, 32.80.Cy, 32.80.Pj

Atomic collisions are essential to the formation of Bose-Einstein condensates (BEC), redistributing energy during evaporative cooling. Collisions can be coherent and reversible, leading to diverse phenomena such as superfluidity [1] and reversible formation of molecules [2] in BECs with a single internal state. When internal degrees of freedom are included (as in spinor condensates), coherent collisions lead to rich dynamics [3,4] in which the population oscillates between Zeeman sublevels. We present the first observation of coherent spin oscillations in a spin-1 condensate with antiferromagnetic interactions (in which the interaction energy of colliding spin-aligned atoms is higher than that of spin-antialigned atoms.)

Spinor condensates have been a fertile area for theoretical studies of dynamics [5–7], ground states [8,9], and domain formation [10]. Extensive experiments on the ferromagnetic $F = 1$ hyperfine ground state of ^{87}Rb demonstrated spin oscillations and coherent control of spinor dynamics [3,11]. The miscibility of components of opposite spin projection in ^{23}Na demonstrated the antiferromagnetic nature of the $F = 1$ ground state [12]. Tunneling across induced spin striations was also studied in ^{23}Na [13]. No spin oscillations have been reported in sodium BEC until now. The $F = 2$ state of ^{87}Rb is likely antiferromagnetic, but a cyclic phase is possible [14,15]. Magnetic control of the amplitude and period of spin oscillations has been demonstrated for this state [4].

At low magnetic fields, spin interactions dominate the dynamics. The different sign of the spin-dependent interaction causes the antiferromagnetic $F = 1$ case to differ from the ferromagnetic one both in the structure of the ground-state magnetic phase diagram and in the spinor dynamics. Both cases can exhibit a regime of slow, anharmonic spin oscillations; however, this behavior is predicted over a wide range of initial conditions only in the antiferromagnetic case [7]. The spin interaction energies in sodium are more than an order of magnitude larger than in ^{87}Rb $F = 1$ for a given condensate density [3], facilitating studies of spinor dynamics.

This Letter reports the first measurement of the ground-state magnetic phase diagram of a spinor condensate, and the first experimental study of coherent spinor dynamics in an antiferromagnetic spin-1 condensate. Both show good agreement with the single-spatial-mode theory [7], which has a well-developed analytic solution for spin-1 condensates. To study the dynamics, we displace the spinor from its ground state, observing the resulting oscillations of the Zeeman populations as a function of applied magnetic field B. At low field the oscillation period is constant and at high field it decreases rapidly. At a critical field the oscillation period diverges, and the amplitude displays a resonance-like feature, all as predicted by theory [7]. These measurements have allowed us to improve by a factor of 5 the determination of the sodium $F = 1$ spin-dependent interaction strength, which is proportional to the difference $a_{f=2} - a_{f=0}$ in the spin-dependent scattering lengths.

The state of the condensate in the single-mode approximation (SMA) is written as the product $\phi(\mathbf{r})\boldsymbol{\zeta}$ of a spin-independent spatial wave function $\phi(\mathbf{r})$ and a spinor $\zeta = (\sqrt{\rho_-}e^{i\theta_-}, \sqrt{\rho_0}e^{i\theta_0}, \sqrt{\rho_+}e^{i\theta_+})$. We use ρ_-, ρ_0, and ρ_+ (θ_-, θ_0, and θ_+) to denote fractional populations (phases) of the Zeeman sublevels $m_F = -1$, 0, and 1, so that $\sum_i \rho_i = 1$. The spinor's ground state and its nonlinear dynamics may be derived from the spin-dependent part of the Hamiltonian in the single-mode and mean-field approximations, subject to the constraints that total atom number N and magnetization $m \equiv \rho_+ - \rho_-$ are conserved [7]. The "classical" spinor Hamiltonian E is a function of only two canonical variables: the fractional population ρ_0 and the relative phase $\theta \equiv \theta_+ + \theta_- - 2\theta_0$. It is given by

$$E = \delta(1 - \rho_0) + c\rho_0[(1 - \rho_0) + \sqrt{(1 - \rho_0)^2 - m^2}\cos\theta], \tag{1}$$

where $\delta = h \times (2.77 \times 10^{10}\ \mathrm{Hz/T^2})B^2$ is the quadratic Zeeman shift [7] with h the Planck constant. (The linear Zeeman shift has no effect on the dynamics.) The spin-

dependent interaction energy is $c = c_2\langle n\rangle$, where $\langle n\rangle$ is the mean particle density of the condensate and $c_2 = 4\pi\hbar^2(a_{f=2} - a_{f=0})/3M$ is the spin-dependent interaction coefficient [7,16]. Here M is the atomic mass. $a_{f=2}$ and $a_{f=0}$ are the s-wave scattering lengths for a colliding pair of atoms of total spin $f = 2$ and $f = 0$, respectively. If c_2 is positive (negative), the system is antiferromagnetic (ferromagnetic). Both the spinor ground state and the spinor dynamics are determined by Eq. (1).

We produce a BEC of 10^5 ^{23}Na atoms in the $F = 1$ state, with an unobservably small thermal fraction, in a crossed-beam 1070 nm optical dipole trap [17]. The trap beams lie in the horizontal xy plane, so that the trap curvature is nearly twice as large along the vertical z axis as in the xy plane. By applying a small magnetic field gradient with the MOT coils (less than 10 mT/m) during the 9 s of forced evaporation, we fully polarize the BEC: all atoms are in $m_F = +1$. Conservation of spin ensures that the magnetization remains constant once evaporation has ceased; a state with $\rho_+ = 1$ persists for the lifetime of the condensate, about 14 s.

We then turn off the gradient field and adiabatically apply a bias field B of 4 to 51 μT along $\hat{x}$, leaving the BEC in the $\rho_+ = 1$ state. To prepare an initial state, we apply an rf field resonant with the linear Zeeman splitting; typically the frequency is tens to hundreds of kilohertz. Rabi flopping in the three-level system is observed [18], and controlling the amplitude and duration of the pulse can produce any desired magnetization m, which also determines the population ρ_0. The flopping time is less than 50 μs, much shorter than the characteristic times for spin evolution. Using this Zeeman transition avoids populating the $F = 2$ state, thus avoiding inelastic losses, which are much greater for ^{23}Na than for ^{87}Rb.

We measure the populations ρ_i of atoms in the three Zeeman sublevels by Stern-Gerlach separation and absorption imaging [17]. The Stern-Gerlach gradient is parallel to the bias field $\vec{B}$, while the imaging beam propagates in the $\hat{z}$ direction. The phase θ is not measured.

To measure the phase diagram of the ground state $m_F = 0$ population as a function of magnetization and magnetic field, we first set the magnetization using the rf pulse. We then ramp the field to a desired final value over 1 s, wait 3 s for equilibration, and image as above.

Figure 1(b) displays the measured ground-state magnetic phase diagram. The theoretical prediction in Fig. 1(a) is the population ρ_0 that minimizes the energy, Eq. (1). Such minima always occur at $\theta = \pi$ for antiferromagnetic interactions. The single-mode theory is justified as none of the images showed spatial structure. The predicted phase diagram was calculated for spin interaction energy $c = h \times 20.5$ Hz (determined by spin dynamics as described below). Measurements agree well with the prediction across most of the phase diagram.

The first, magnetic field dependent term of Eq. (1) tends to maximize the equilibrium ρ_0 population, while the second, spin-dependent, term tends to minimize ρ_0 for the antiferromagnetic case. The phase transition indicated by the thick line in Fig. 1(a) arises where these opposing tendencies cancel for $\rho_0 = 0$. Along the transition contour, ρ_0 rapidly falls to zero. By contrast, the ferromagnetic phase diagram has $\rho_0 = 0$ only at $m = 1$. In the region $B < 15$ μT and $m > 0.6$, there should be virtually no population in $m_F = 0$ for antiferromagnetic interactions, and populations up to $\rho_0 = 0.34$ for ferromagnetic interactions (assuming the same magnitude of c). For our equilibrium data, the reduced χ^2 with respect to the antiferromagnetic (ferromagnetic) prediction in this region is 2 (20). This confirms that sodium $F = 1$ spin interactions are antiferromagnetic [12].

Across most of the phase diagram, the scatter in the population is consistent with the density variations expected from the measured shot-to-shot variation in atom number. The variance of results is not due to the magnetic field (calibrated to a precision of 0.2 μT), nor to residual field variations across the BEC (less than 250 pT).

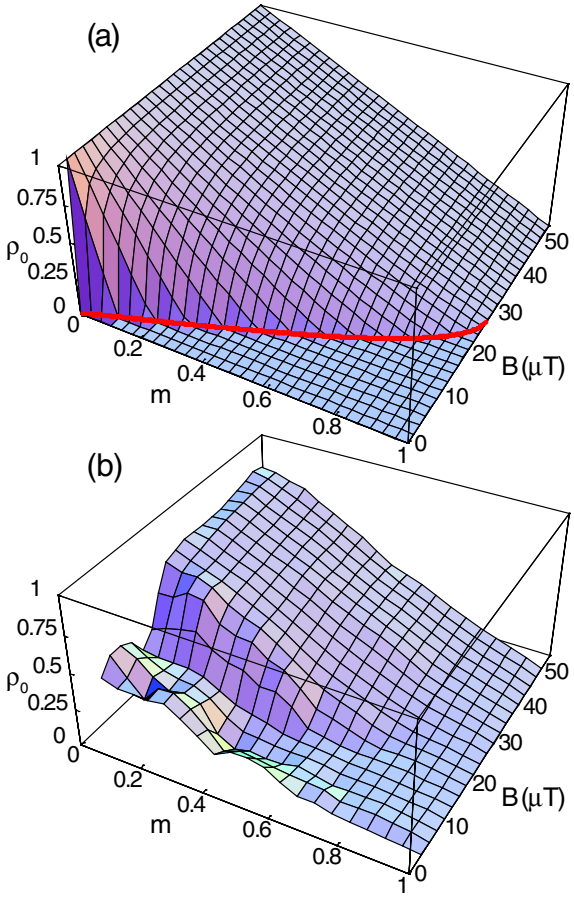

FIG. 1 (color online). (a) Theoretical prediction of the ground-state fractional population ρ_0 as a function of magnetization m and applied magnetic field B, assuming a spin-dependent interaction energy $c = h \times 20.5$ Hz. The thick line lying in the $\rho_0 = 0$ plane indicates the boundary between the $\rho_0 = 0$ and the $\rho_0 > 0$ regions. (b) Measurement.

Uncertainties in setting the magnetization are obviated, as the magnetization is measured for each point as the difference in fractional populations $m = \rho_+ - \rho_-$. The measured populations agree well with the predictions, except for the low-field low-magnetization region. There the system has not fully equilibrated to the ground state, and the measurements show greater variance. We observe equilibration times (see below) ranging from 200 ms at high fields to several seconds at low fields, by which time atom loss is substantial.

If the spinor is driven away from equilibrium, the full coherent dynamics of the system Eq. (1) are revealed. We initiate the spinor dynamics with the rf pulse as above, but now observe evolution over millisecond time scales.

The spinor dynamics are described by the Hamilton equations for Eq. (1) [7]:

$$\dot{\rho}_0 = -\frac{2}{\hbar}\frac{\partial E}{\partial \theta} \quad \text{and} \quad \dot{\theta} = \frac{2}{\hbar}\frac{\partial E}{\partial \rho_0}. \tag{2}$$

The system is closely related to the double-well "bosonic Josephson junction" (BJJ) [19,20] and exhibits a regime of small, harmonic oscillations and, near a critical field B_c, is predicted to display large, anharmonic oscillations. At B_c the period diverges (where $\delta(B_c) = c[(1-\rho_0) + \sqrt{(1-\rho_0)^2 - m^2}\cos\theta]$, with ρ_0 and θ taken at $t = 0$) [7]. The critical value corresponds to a transition from periodic-phase to running-phase solutions of Eq. (2). At the critical value it is predicted that the population is trapped in a spin state with $\rho_0 = 0$, a phenomenon similar to the macroscopic quantum self-trapping observed in the BJJ [20]. However, very small fluctuations in magnetic field or density will drive ρ_0 away from 0. Observing a tenfold increase in the period above its zero-field value would require a technically challenging magnetic field stability of better than 100 fT.

Figure 2 plots the period and amplitude of oscillation as a function of magnetic field. An example of the oscillating populations is shown in the inset. The spinor condensate is prepared with initial $\rho_0 = 0.50 \pm 0.01$ [21] and $m = 0.00 \pm 0.02$, and a plot of ρ_0 versus time is taken at each field value. Qualitatively, the period is nearly independent of magnetic field at low fields, with a small peak near $B_c = 28\ \mu$T, followed by a steep decline in period. The amplitude likewise shows a maximum at B_c. Oscillations are visible over durations of 40 to 300 ms. Beyond these times, the amplitude of the shot-to-shot fluctuations in ρ_0 is roughly equal to the harmonic amplitude. This indicates dephasing due to shot-to-shot variation in oscillation frequency, probably associated with the variations in magnetic field and condensate density, rather than any fundamental damping process. At even longer times, we observe damping and equilibration to a new constant ρ_0; the damping time varies with magnetic field from 200 ms to 5 s.

For the theoretical prediction in Fig. 2, the initial values of ρ_0 and m are obtained experimentally. We treat only c and $\theta(t = 0)$ as free parameters; c is also predicted by prior determinations of c_2 and our knowledge of the condensate density. The initial relative phase is *not* the equilibrium value $\theta = \pi$, due to our rf preparation. For a three-level system driven on resonance and starting with all atoms in $m_F = +1$, the relative phase is $\theta = 0$ at all times during the rf transition, as we derive from Ref. [18].

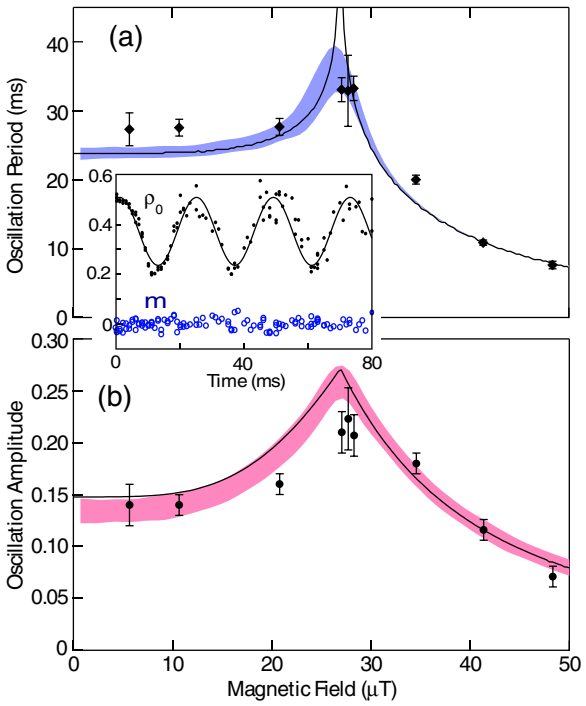

FIG. 2 (color online). Period (a) and amplitude (b) of spin oscillations as a function of applied magnetic field, following a sudden change in spin state. Solid lines are predictions from solving Eq. (2). The theoretical prediction of the period diverges at about 27 μT. Shaded regions are ± 1 standard deviation about the mean values (from Monte Carlo simulation, see text.) Inset: Fractional Zeeman population (solid dots) and magnetization (open circles) as a function of time after the spinor condensate is driven to $\rho_0 = 0.5$, $m = 0$. $B = 6.1\ \mu$T. The solid line is a sinusoidal fit.

The best fit to the data in Figs. 2(a) and 2(b) is obtained by using $c = h \times (21 \pm 2)$ Hz and $\theta(t = 0) = 0.5 \pm 0.3$ (with no other free parameters). Deviation from $\theta(t = 0) = 0$ could be due to state preparation: a fraction of only 2% in the $m_F = -1$ level before the rf pulse can produce the observed deviation after the pulse. Away from the critical field B_c, agreement with theory is good. The fitted value of c implies that B_c is 27 μT, in reasonable agreement with the apparent peak observed at 28 μT. Our ability to observe strong variations in period near B_c is limited by density fluctuations (8%) and magnetic field fluctuations (0.2 μT). Near B_c typically only one cycle is visible before dephasing is complete. Such rapid dephasing can, itself, be taken as evidence of a strongly B-dependent period, as expected near the critical field.

To include the known fluctuations in density and magnetic field in our model, we perform a Monte Carlo simu-

lation of the expected signal, based on measured, normally distributed shot-to-shot variations in values of c, δ, m, and $\rho_0(t=0)$. At each value of B in Fig. 2, we simulate 80 time traces, with each point in the time trace determined from Eq. (2). We fit sine waves to the simulated traces and record the mean and standard deviation of their amplitude and period. The results (shaded in Fig. 2) show a less sharp peak in the period. The smoothing of the peak at B_c is consistent with our data.

It is clear in Fig. 2 that the oscillation period is insensitive to the magnetic field at low values of the field. In this regime, the period is sensitive only to the spin interaction c_2 and the density of the condensate $\langle n \rangle$. Measuring this period allows us to determine the difference in scattering lengths $a_{f=2} - a_{f=0}$. The trace inset in Fig. 2 was taken in this regime, at a magnetic field of $B = 6.1\ \mu$T, and shows harmonic oscillations with period 24.6 ± 0.3 ms. Here the predicted period dependence on magnetic field, $14\ \mu\text{s}/\mu\text{T}$, is indeed weak and the oscillations dephase only slightly over the duration shown. Using this measurement of the period [in which much more data was taken than for each point making up Figs. 2(a) and 2(b)] and including uncertainties in initial θ, ρ_0, and m, we obtain the spin interaction energy $c = h \times (20.5 \pm 1.3)$ Hz.

Finding $a_{f=2} - a_{f=0}$ requires a careful measurement of the condensate density. We take absorption images with various expansion times to find the mean field energy. The images yield the column density in the xy plane, and the distribution in the z direction can be inferred from our trap beam geometry. We find that the mean density of the condensate under the conditions of the inset to Fig. 2 is $\langle n \rangle = 8.6 \pm 0.9 \times 10^{13}\ \text{cm}^{-3}$. From this we calculate $a_{f=2} - a_{f=0} = (2.47 \pm 0.27)a_0$, where $a_0 = 52.9$ pm is the Bohr radius. This is consistent with a previous measurement, from induced spin striations, of $a_{f=2} - a_{f=0} = (3.5 \pm 1.5)a_0$ [12] and is smaller than the difference between scattering lengths determined from molecular levels, $a_{f=2} = (55.1 \pm 1.6)a_0$ and $a_{f=0} = (50.0 \pm 1.6)a_0$ [22]. A multichannel quantum defect theory calculation gives $a_{f=2} - a_{f=0} = 5.7a_0$ [23].

Finally, we consider the validity of the spatial single-mode approximation. Spatial degrees of freedom decouple from spinor dynamics when the spin healing length $\xi_s = 2\pi\hbar/\sqrt{2m|c_2|n}$ is larger than the condensate. Experiments on ^{87}Rb with one Thomas-Fermi (TF) radius larger than ξ_s displayed several cycles of single-mode spin oscillation before domains formed [3]. From our density measurements we find TF radii of $(9.4, 6.7, 5.7)\ \mu$m. The spin healing length is $\xi_s = 17\ \mu$m; spatial structure formation should be suppressed. Furthermore, condensates with antiferromagnetic interactions are predicted not to form domains [10,24]. These predictions are confirmed: Stern-Gerlach absorption images show three components with identical spatial distributions after ballistic expansion, even after several seconds of evolution.

In conclusion, we have studied both the ground state and the spinor dynamics of a sodium $F = 1$ spinor condensate. Both agree well with theoretical predictions in the SMA. By measuring the spin oscillation frequency at low magnetic field, we have determined the difference in spin-dependent scattering lengths. The observed peak in oscillation period as a function of magnetic field demonstrates that the spinor dynamics are fundamentally nonlinear. It also suggests the existence of the predicted regime of highly anharmonic spin oscillations at the center of this peak, which should be experimentally accessible with sufficient control of condensate density and magnetic field. Observation of anharmonic oscillations, as well as population trapping and spin squeezing, could be aided by a minimally destructive measurement of spin projection [25] to reduce the effects of magnetic field drifts and shot-to-shot density fluctuations.

We thank W. Phillips for helpful discussions, and ONR and NASA for support. A. T. B received financial support from the NRC. L. D. T. received support from the Australian-American Fulbright Commission.

[1] M. R. Matthews *et al.*, Phys. Rev. Lett. **83**, 2498 (1999).
[2] E. A. Donley *et al.*, Nature (London) **417**, 529 (2002).
[3] M.-S. Chang *et al.*, Nature Phys. **1**, 111 (2005).
[4] J. Kronjäger *et al.*, Phys. Rev. Lett. **97**, 110404 (2006).
[5] M. Moreno-Cardoner *et al.*, Phys. Rev. Lett. **99**, 020404 (2007).
[6] C. K. Law, H. Pu, and N. P. Bigelow, Phys. Rev. Lett. **81**, 5257 (1998).
[7] W. Zhang *et al.*, Phys. Rev. A **72**, 013602 (2005).
[8] T.-L. Ho, Phys. Rev. Lett. **81**, 742 (1998).
[9] W. Zhang, S. Yi, and L. You, New J. Phys. **5**, 77 (2003).
[10] W. Zhang *et al.*, Phys. Rev. Lett. **95**, 180403 (2005).
[11] J. Kronjäger *et al.*, Phys. Rev. A **72**, 063619 (2005).
[12] J. Stenger *et al.*, Nature (London) **396**, 345 (1998).
[13] D. M. Stamper-Kurn *et al.*, Phys. Rev. Lett. **83**, 661 (1999).
[14] A. Widera *et al.*, New J. Phys. **8**, 152 (2006).
[15] T. Kuwamoto *et al.*, Phys. Rev. A **69**, 063604 (2004).
[16] D. M. Stamper-Kurn and W. Ketterle, in *Coherent Atomic Matter Waves*, edited by R. Kaier *et al.* (Springer, New York, 2001), p. 137; arXiv:cond-mat/0005001.
[17] R. Dumke *et al.*, New J. Phys. **8**, 64 (2006).
[18] M. Sargent and P. Horwitz, Phys. Rev. A **13**, 1962 (1976).
[19] S. Raghavan *et al.*, Phys. Rev. A **59**, 620 (1999).
[20] M. Albiez *et al.*, Phys. Rev. Lett. **95**, 010402 (2005).
[21] All uncertainties in this paper are 1 standard deviation combined statistical and systematic uncertainties.
[22] A. Crubellier *et al.*, Eur. Phys. J. D **6**, 211 (1999).
[23] J. P. Burke, C. H. Greene, and J. L. Bohn, Phys. Rev. Lett. **81**, 3355 (1998).
[24] N. P. Robins *et al.*, Phys. Rev. A **64**, 021601 (2001).
[25] G. A. Smith *et al.*, Phys. Rev. Lett. **93**, 163602 (2004).